J. Fluid Mech. (1983), *vol.* 127, *pp.* 429–442
Printed in Great Britain

Estimation of pressure fields in combustion of vapour clouds

By F. A. WILLIAMS
Department of Mechanical and Aerospace Engineering, Princeton University, New Jersey

(Received 3 June 1982)

A simplified model is developed for the dynamics of pressure fields supported by deflagrations in open axisymmetric configurations. The model employs overall conservation of mass, laws of flame propagation, overall conservation of momentum and a statement of conservation of mass and momentum across a shock that precedes the flame. The model represents an improvement over an earlier model in a number of respects, notably in allowing pressures at the flame and at the shock to differ. Explicit results for time histories are obtained by an expansion method for small values of the Mach number of flame propagation. The model may be employed to estimate overpressures that may develop subsequent to ignition of flat vapour clouds.

1. Introduction

An earlier publication (Williams 1976; hereinafter referred to as I) addressed the problem of obtaining simple estimates for pressures encountered when a deflagration propagates through an unconfined combustible in a configuration more complex than that of planar, cylindrical or spherical symmetry. Relevant literature has been cited in I and will not be recited here. The work in I produced a model capable of providing order-of-magnitude estimates of pressures in axisymmetric configurations. To aid in the estimation of damage from explosions of unconfined vapour clouds it is desirable to develop improved models having better accuracies. The study reported herein defines an improved model and draws conclusions concerning its accuracy and its potential applications. As in I, the philosophy of the approach has been to introduce as little detail of the physics as possible, consistent with being able to calculate the quantities of interest.

2. Description of model

An axisymmetric configuration is considered in which there is a thin shock at radius R and a thin flame at radius r, with $r < R$. These flame and shock surfaces may be concentric spheres or concentric cylinders. For ground-level initiation of a uniform cloud of initial height h, the spherical approximation is employed until the flame breaks through the top of the cloud, and the cylindrical approximation is employed thereafter. In the cylindrical case the shock extends into the inert gas above the cloud, in a manner to be defined later (see appendix A). The flame is presumed to propagate at a prescribed burning velocity S with respect to the combustible ahead of it. Although the model allows S to vary with time t, the difficult problem of calculating the turbulent burning velocity is not addressed.

The model in I postulated a spatially constant pressure throughout the gas enclosed by the shock. Although this is not too unrealistic for sufficiently high Mach numbers

of flame propagation, the overpressure at the flame may exceed that at the shock by orders of magnitude at lower flame Mach numbers. Therefore it is of interest to modify the model by allowing the pressure p just behind the shock to differ from the pressure P just ahead of the flame. In selecting a pressure scale herein, ambient pressure is assigned the value unity. The present model may be termed a two-pressure model, in contrast with the one-pressure model in I.

Overall conservation principles will be introduced and employed to calculate histories of R, p, r and P.

3. Conservation laws

3.1. *Shock relations*

It is convenient although not essential to use the initial shock radius R_0 and the Newtonian sound speed a_0 of the undisturbed gas for defining non-dimensional variables, as in I. The definitions of I, $x = r/R_0$, $y = R/R_0$, $s = S/a_0$ and $\tau = a_0 t/R_0$, are then introduced. The statement in I of conservation of mass and momentum across the shock is then written as

$$p = 1 + (1-\kappa)\left(\frac{dy}{d\tau}\right)^2, \tag{1}$$

where κ denotes the ratio of the density of the undisturbed gas to the density just behind the shock. According to shock relations for an ideal gas,

$$\kappa = \frac{(\gamma-1)p + (\gamma+1)}{(\gamma-1) + (\gamma+1)p}, \tag{2}$$

where γ denotes the ratio of specific heats. Contary to the situation in I, the greater freedom of the two-pressure model favours use of (2) in all cases.

3.2. *Overall mass conservation*

The ratio K of the ambient density to the density of the gas just ahead of the flame is related to κ by the assumption that isentropic conditions with constant γ prevail between the shock and the flame, i.e.

$$K = \kappa\left(\frac{p}{P}\right)^{1/\gamma}. \tag{3}$$

The approximate statement in I of overall mass conservation may be improved by employing an average between K^{-1} and κ^{-1} for the density of the shocked but unburnt gas. For the axisymmetric configuration the formula in I for overall mass conservation involves the relief efficiency η of the shock pattern above the cloud, introduced to account for the influence of these shocks on the mass balance. An alternative definition of η and a discussion of its interpretation are given in appendix A. Equating the sum of the mass in the cylinder and the hemisphere above it to the initial value of this sum, we find in non-dimensional variables that

$$jz + \tfrac{1}{2}(y^j - x^j)(K^{-1} + \kappa^{-1}) + \frac{2y}{3\alpha}\eta y^j \tfrac{1}{2}(K^{-1} + \kappa^{-1}) = y^j + \frac{2y}{3\alpha}\eta y^j, \tag{4}$$

where $\alpha = h/R_0$. Here z, a non-dimensional measure of the mass of burnt gas, is defined as the ratio of the density of the burnt gas to ambient density, multiplied by x^j/j. In the axisymmetric problem $j = 2$; the spherical case applicable prior to flame breakthrough is recovered by putting $j = 3$ and $\eta = 0$.

3.3. *Equation for flame spread*

The density of the burnt gas may be related to P through the ideal-gas law. For this purpose, let θ denote the product of three factors: the ratio of the ambient temperature to the temperature of the burnt gas, the ratio of the mean molecular weight of the burnt gas to the mean molecular weight of the ambient gas, and the ratio of the pressure behind the deflagration to the pressure just ahead of it. Although the first of these three factors is the dominant contributor to θ and causes it to be of order 10^{-1}, the second and third may account for generally small decreases of molecular weight and pressure across the deflagration, thereby providing small corrections to the formulation in I. With this definition of θ, it is seen that

$$z = \theta P x^j / j, \tag{5}$$

in terms of which the non-dimensional form of the equation for the rate of engulfment of combustible by the flame (i.e., the mass balance for the burnt gas) may be written as

$$\frac{dz}{d\tau} = \frac{x^{j-1} s \beta}{K}. \tag{6}$$

Equation (6) also represents an improvement over the corresponding formula in I in that a factor β has been introduced to account for horizontal motion of the gas behind the flame as a consequence of upward expansion of hot products, including effects of buoyancy. The evaluation of β is discussed in appendix B.

3.4. *Conservation of momentum in the unburnt gas*

Because of the additional degree of freedom introduced by allowing P and p to differ, an additional conservation law is needed, beyond those introduced in I. Since pressure-field variations between the shock and the flame are responsible for differences between P and p, it is logical to introduce a statement of overall momentum conservation for the shocked but unburnt gas as the additional conservation principle. The formulation of this momentum conservation is developed in appendix C. The results are conveniently expressed in terms of the non-dimensional measure m of the momentum of the shocked but unburnt gas, defined in (C 2). The conservation law, obtained from (C 1) with terms of order s^2 neglected, is

$$\frac{dm}{d\tau} = (P-1)\, x^{j-1} + [\tfrac{1}{4} j (P-1) + (1 - \tfrac{1}{4} j)\,(p-1)]\,(y^{j-1} - x^{j-1}). \tag{7}$$

In terms of other variables, it is seen from appendix C that m may be expressed as

$$m = (y-x)\left\{a x^{j-1} \frac{\beta s}{K} [(K\theta P)^{-1} - 1] + (1-a)\, y^{j-1} \frac{[(p-1)\,(1-\kappa)]^{\frac{1}{2}}}{\kappa}\right\}, \tag{8}$$

where a is a weighting factor for the contribution of the momentum just ahead of the flame to m. Equation (8) expresses m as a weighted average of the momentum at the flame and at the shock. Although the value $a = \frac{1}{2}$ seems reasonable, it will be found by studying the limit of small s that a correction to this value is desirable if $\eta \neq 0$.

3.5. *Summary of the problem*

Equations (1)–(8) may be viewed as expressions for y, κ, K, x, p, z, m and p with γ, s, θ, η, α, β, a and j given. Since there are three first-order differential equations in the system, initial values for z and m are needed, in addition to the initial value

$y = 1$. Although eliminations of some of the variables are readily achieved, derivation of results with the generality attained in I is not feasible. Therefore attention is restricted to 'quasi-steady' (or self-similar) solutions and to time-dependent behaviours for small flame Mach numbers s.

4. Self-similar solutions

From I it may be inferred that at late times the system tends to approach a self-similar behaviour. Self-similar solutions may be derived by beginning with the assumptions that P, p and y/x remain constant, independent of τ. With γ constant, it follows from (2) and (3) that κ and K also remain constant. The self-similar solutions apply when s, β, a and θ are constant, whence z/x^j is constant according to (5), and $\mu \equiv \eta y/\alpha$ must then be constant, according to (4), as has been found and discussed in I. From (1) it is found that y increases linearly with τ, viz $y = 1 + c\tau$, where $c = [(p-1)/(1-\kappa)]^{\frac{1}{2}}$. The constancy of y/x then implies that x is proportional to $1 + c\tau$, and (5) and (8) respectively then show that z and m are proportional to $(1 + c\tau)^j$. Use of these results in (6) and (7) demonstrates that

$$\frac{m}{z} = \frac{K}{\beta s}\left\{(P-1) + [\tfrac{1}{4}j(P-1) + (1-\tfrac{1}{4}j)(p-1)]\left[\left(\frac{y}{x}\right)^{j-1} - 1\right]\right\}. \tag{9}$$

Finally, from (1), $dy^j/d\tau = cjy^{j-1}$, which when divided by (6) produces

$$\frac{y^j}{z} = j\left(\frac{y}{x}\right)^{j-1}\frac{K}{\beta s}\left[\frac{p-1}{1-\kappa}\right]^{\frac{1}{2}}. \tag{10}$$

The algebraic equations that describe the self-similar behaviour are (2)–(5) and (8)–(10); they serve to determine p, P, κ, K, y/x, z/x^j and m/x^j as functions of γ, s, θ, μ, β, a and j. Through various substitutions the system may be reduced to two simultaneous nonlinear equations for the two unknowns p and P, which may be solved by trial and error.

Because of the large number of parameters involved, a parametric study like that reported in I has not been performed for the present self-similar solutions. Instead, a comparison was made of predictions of the models for a representative case, as shown in figure 1. The value selected for βs corresponds to a relatively large burning velocity, of the order of 20–30 m/s; at lower burning velocities predicted overpressures are reduced, roughly in proportion to $(\beta s)^2$. In generating results for the two-pressure model in figure 1, the formula $a = \frac{1}{2}[1 + \frac{2}{3}(\eta/\alpha)\, y]^{-1}$ was employed in (8), as derived in § 5.

The dashed lines in figure 1 represent the self-similar predictions of the present model. The upper dashed line is the overpressure at the flame, $P-1$, and the lower dashed line that at the shock, $p-1$. The horizontal lines correspond to the spherical solution (with $j = 3$ and $\eta = 0$); for weak ignitions they represent upper bounds of overpressures. These bounds are close to those of the more-exact similarity solutions (Kuhl 1981), e.g. for $S = 20$ m/s in the spherical case, the present value of 0·22 for the overpressure at the flame is to be compared with 0·265. The vertical line defines the condition for the flame to break through the top of the cloud, as given by (B 1). The curves showing the axisymmetric solutions are most relevant at values of R/h greater than that of flame breakthrough. If η and βs remain constant then, as R/h increases, the self-similar overpressures decrease as shown. The shock radius is found to be 2·24 times the flame radius in this example.

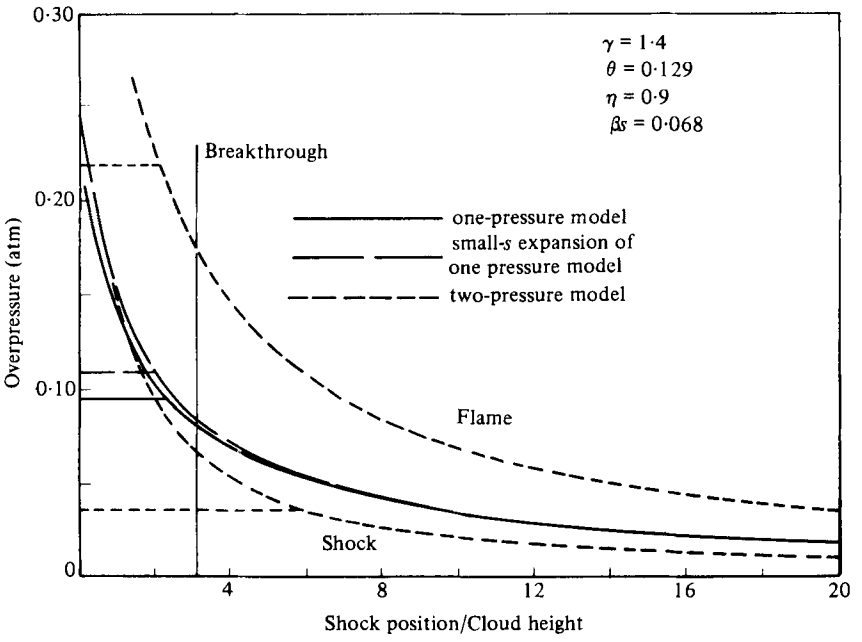

FIGURE 1. Overpressures as functions of the ratio of the shock position to the cloud height for various self-similar models.

The solid curves in figure 1 are the self-similar predictions of the model published in I, with (2) employed for κ. This model provides only one overpressure, which is seen to fall between the shock and flame overpressures of the present model. Thus, if only order-of-magnitude estimates of pressures are desired, the simpler model in I seems adequate. If peak pressures must be calculated then the present, two-pressure model seems better.

Shown departing from the solid curve in figure 1 at the smaller values of R/h is a dashed curve labelled 'small-s expansion'. This curve is obtained from the self-similar version of a development for the one-pressure model analogous to the development given in the following section for the two-pressure model. It is seen in figure 1 that, even at this relatively large value of βs, the expansion provides overpressure accuracies better than 15 %. This suggests that the simplifications to be derived in § 5 produce results with good accuracy in the situations of greatest practical interest.

5. Simplifications for small Mach numbers of flame propagation

In the majority of the applications s is a small parameter. This observation has prompted research based on acoustics. The acoustic studies, which involve the solution of partial differential equations, are particularly worthwhile when asymptotic solutions admitting weak shocks are employed (Chiu, Lee & Knystautas 1977). However, for asymmetrical configurations this approach has not yet properly considered the presence of a deflagration enclosed by a shock, and is not yet sufficiently well developed to be compared with the present method. To facilitate future comparisons and applications of the present results, it is of interest to develop the

small-s limit of the theory. Formal expansions of (1)–(8) for small values of s provide significant simplifications that enable analytical solutions to be obtained. These solutions are derived here and are used in §6 to discuss time-dependent behaviour.

When s is small both $P-1$ and $p-1$ are small if these assumptions are consistent with the initial conditions. Therefore we put $P = 1+\epsilon$ and $p = 1+\delta$, and treat ϵ and δ as small quantities. From the expansion of (2), $\kappa = 1-\delta/\gamma$, and therefore the solution to the expansion of (1) is

$$y = 1+\gamma^{\frac{1}{2}}\tau. \tag{11}$$

With ϵ small, the expansion of (5) gives $z = \theta x^j/j$ in the first approximation, and, since the expansion of (3) is $\kappa = 1-\epsilon/\gamma$, the first approximation to (6) is $dx/d\tau = s\beta/\theta$ if θ remains constant. Therefore

$$x = x_0 + \int_0^\tau \frac{s\beta}{\theta}\, d\tau, \tag{12}$$

where x_0 is the value of x at $\tau = 0$. Equation (12) allows s to be a prescribed function of τ. From (11) and (12) it is seen that the motions of the (weak) shock and of the flame are known in advance and are continuous. Self-similar solutions may be recovered from (11) and (12) by letting s be constant and by putting $x_0 = s\beta/\theta\gamma^{\frac{1}{2}}$, obtaining $x/y = s\beta/\theta\gamma^{\frac{1}{2}} =$ constant.

The functions $\epsilon(\tau)$ and $\delta(\tau)$ are obtained from expansions of (4), (7) and (8). Use of the expansions for P, p, κ and K in (8) shows that, for small ϵ and δ,

$$m = (y-x)\left[(1-a)\, y^{j-1}\frac{\delta}{\gamma^{\frac{1}{2}}}(1+O\{\delta\}) + a x^{j-1}\frac{s\beta}{\theta}(1-\theta)(1+O\{\epsilon,\delta\})\right], \tag{13}$$

where O defines the orders of neglected terms. In view of (12), (7) can be written exactly as

$$\frac{s\beta}{\theta}\frac{dm}{dx} = \epsilon x^{j-1} + [\tfrac{1}{4}j\epsilon + (1-\tfrac{1}{4}j)\,\delta](y^{j-1}-x^{j-1}). \tag{14}$$

The expansion of (4) to first order in ϵ and δ can be shown to be

$$x^j(1-\theta) = y^j\left[1+\frac{2\eta}{3\alpha}y\right]\frac{\epsilon+\delta}{2\gamma}(1+O\{\epsilon,\delta\}). \tag{15}$$

Equations (13)–(15) possess solutions consistent with the assumption that δ is of higher order than ϵ in the small parameter $s\beta/\theta$, provided that a is suitably chosen. Equations (11) and (12) show that, for sufficiently large τ, x/y is of order $s\beta/\theta$. Given suitable initial conditions, x/y is always of this order; consideration is restricted to such cases. Then (15) shows that ϵ is of order $(s\beta/\theta)^j$. Since $(x/y)^{j-1}\, s\beta/\theta$ is of order $(s\beta/\theta)^j$, the first term in the square brackets in (13) is of higher order than the second when δ is of higher order than ϵ. Since ϵ and δ both are of higher order than x/y, a two-term expansion of (13) is

$$m = (y-x)\, x^{j-1} a\frac{s\beta}{\theta}(1-\theta) + (1-a)\, y^j\frac{\delta}{\gamma^{\frac{1}{2}}}. \tag{16}$$

When this result is substituted into (14) and an order-of-magnitude analysis is performed, it is found that the dominant higher-order terms occur on the left-hand side and that δ is of order $(s\beta/\theta)^{j+1}$, provided that the selected weighting a causes an identity to occur in the lowest order.

With the anticipated relative ordering of ϵ and δ, the result

$$P-1 \equiv \epsilon = \frac{2\gamma(1-\theta)\left(\frac{x}{y}\right)^j}{1+\frac{2\eta}{3\alpha}y} \tag{17}$$

is obtained in the first approximation. The calculation of δ is more complicated, and entails employing (16) in (14). If μ is constant, then to lowest order

$$a = \frac{1}{2}\left[1+\frac{2\eta}{3\alpha}y\right]^{-1} \tag{18}$$

results from the substitution and expansion. The consequent η-dependent weighting for the momentum appears physically reasonable in view of possible influences of the shocked non-combustible on the momentum of the shocked combustible. Carrying the expansion to second order, using (15) and (18), yields under self-similar conditions

$$\delta = \frac{\left[ja\left(\frac{s\beta}{\theta}\right)^2(1-\theta)+(1-\frac{1}{4}j)\epsilon\right]\left(\frac{x}{y}\right)^{j-1}}{j(1-a)-(1-\frac{1}{2}j)}, \tag{19}$$

in which ϵ refers to the first approximation given in (17). For $j = 3$ the ϵ term in (19) is of higher order and should be omitted; for $j = 2$ it must be retained. With $j = 3$ we have $a = \frac{1}{2}$, and (19) is

$$p-1 = \tfrac{3}{4}\gamma(1-\theta)\left(\frac{x}{y}\right)^4; \tag{20}$$

with $j = 2$, (19) is

$$p-1 = \frac{2\gamma(1-\theta)\left(\frac{x}{y}\right)^3}{1+\frac{4\eta}{3\alpha}y}. \tag{21}$$

Pressure–time histories may be calculated from (17), (20) and (21) by employing (11) and (12) for y and x. These calculations may be performed for both spherical and axisymmetric propagation, the transition between the two being defined by (B 1). They also may be performed subsequent to complete burnout of a centrally ignited axisymmetric cloud by setting $x = x_c$ = constant, while y is still given by (11). If the initial radius of the cloud is R_c and if the burnt gas is assumed to be spherical in shape, then a mass balance at burnout gives

$$x_c = \frac{R_c^{\frac{2}{3}}h^{\frac{1}{3}}}{R_0}\frac{(\frac{3}{4})^{\frac{1}{3}}}{(P\theta)^{\frac{1}{3}}}, \tag{22}$$

where P is calculated from the axisymmetric solution at burnout. For very flat clouds the formula $x_c = (R_c/R_0)/(P\theta)^{\frac{1}{3}}$ may be better than (22). Pressure decays after burnout are given by (17) and (21) with these values of x_c.

6. Time-dependent solutions

The prescription given in §5 is readily employed to calculate time-dependent solutions without invoking self-similar hypotheses. Results of a representative calculation of this type are shown in figure 2. The initial conditions selected for the

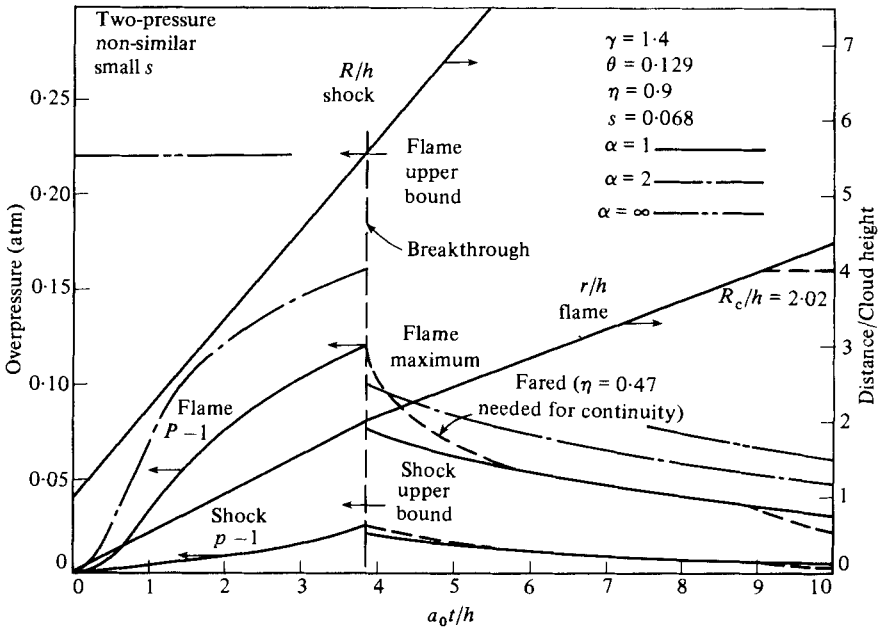

FIGURE 2. Overpressures, shock position and flame position as functions of time, on the basis of an expansion for small Mach numbers of flame propagation.

solid curves in this figure were $r_0 = 0$ and $R_0 = h$. Flame overpressures also are shown for $r_0 = 0$, $R_0 = \frac{1}{2}h$ ($\alpha = 2$) and for $r_0 = 0$, $R_0 = 0$ ($\alpha = \infty$). The upper bounds indicated for the flame and shock overpressures were obtained from the self-similar spherical solution.

It is evident from figure 2 that for the initial conditions selected self-similar conditions are not attained unless $R_0 = 0$. During spherical propagation the overpressures generally increase with time. When $r_0 = 0$ the overpressure at the flame initially increases cubically with time and that at the shock as the fourth power. Breakthrough occurs well before the self-similar pressures are reached.

The equations predict discontinuities in pressures at breakthrough. Such discontinuities are inherent in all of the simplified models that have been considered. In figure 2 if η were made to increase rapidly from 0·47 at breakthrough to 0·9, then the discontinuity in P would be eliminated, and a curve like that labelled 'fared' would be obtained for $P-1$. Although fundamental justification for the variation in η can be devised, it would be complicated to augment the model in a manner that eliminates both of the pressure discontinuities at breakthrough. The discontinuities usually are small and can be smoothed arbitrarily by hand, as has been done in the dashed curves. All smoothing must be done after breakthrough because modifications to the spherical solution by pressure release cannot occur sooner.

The solid curves after breakthrough in figure 2 are those calculated for continued flame propagation. They exhibit slowly decaying pressures as a consequence of increasing upward relief with η constant. The dashed curves beginning at $\tau = 9$ show cessation of flame travel and enhanced pressure decay, calculated to occur after burnout if the cloud radius is $R_c = 2{\cdot}02h$. For clouds with larger values of R_c/h this decay begins proportionally later. Figure 2 is non-dimensional and may be employed for any value of h.

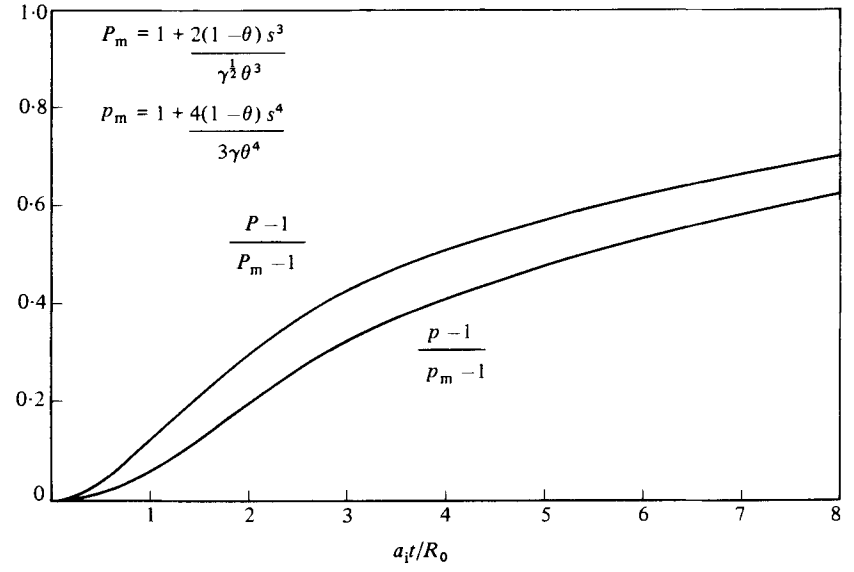

FIGURE 3. Universal curves of transient pressure build-up at the flame and at the shock, for spherically symmetrical conditions within the context of the expansion for low Mach numbers of flame propagation.

Peak overpressures achieved are of particular interest. They generally occur during spherical propagation and are influenced more strongly by initial conditions and by cloud heights than are post-breakthrough pressures. From (11), (12) (with $\beta = 1$), (17) (with $j = 3$, $\eta = 0$) and (20), overpressures during the spherical stage are readily obtained as functions of initial conditions.

The initial value $x_0 = 0$ is realistic for most ignition sources, and gives $y/x = a_i\theta/S + R_0\theta/St$, where $a_i = \gamma^{\frac{1}{2}}a_0$ is the isentropic sound speed. Use of this result in (17) and (20) enables universal pressure–time curves to be plotted for the transient spherical solution. These curves are shown in figure 3, where P_m and p_m identify self-similar values. It is seen from figure 3 that the maximum overpressures $P_m - 1$ and $p_m - 1$ are approached rather slowly with increasing t. The peak is achieved at breakthrough, which occurs at $t \approx h\theta^{\frac{2}{3}}/S$.

The peak value of $P-1$ is

$$\frac{P_m - 1}{\left[1 + \frac{R_0}{h}\frac{s}{\gamma^{\frac{1}{2}}\theta^{\frac{2}{3}}}\right]^3},$$

which is roughly proportional to s^3 but also depends significantly on R_0/h. The self-similar value of the peak $P-1$ is achieved if $R_0/h = 0$, and the peak decreases as R_0/h increases. In figure 2, if R_0/h is decreased then there is no significant modification of the time coordinate, but overpressures are rescaled to have higher peak pressures and earlier inflexions, as may be seen by comparing the curves for $\alpha = 1$ and 2.

The sensitivity of the achieved overpressure to R_0/h emphasizes the importance of the initiation conditions. It is difficult to estimate R_0 accurately for most initiation mechanisms. The occurrence of R_0/h as the relevant parameter implies that for a given initiation mechanism the peak overpressure will increase with increasing cloud height. The self-similar values, written in figure 3, provide conservative estimates of peak

overpressures that are not likely to be too low under any circumstances other than an explosive initiation that produces $r > RS/a_i\theta$ during an early portion of the history.

7. Conclusions

We have demonstrated that it is possible to develop a simplified model for the combustion of axisymmetric vapour clouds that distinguishes between the pressure at the flame and the pressure behind the shock. Simple, analytical results for time histories of pressure fields are obtainable from the model in terms of an expansion for small Mach numbers of flame propagation. The results afford the possibility of calculating the pressure development subsequent to ignition of pancake-shaped clouds of combustible gases. The approach is much quicker than alternative procedures, such as numerical integration of partial differential equations, and moreover it affords the possibility of developing parametric results at low cost. However, some uncertainties remain concerning accuracies of predictions, and therefore it would be of interest to compare selected results with those of more laborious calculations.

There are aspects of the present model that deserve further study. It would be of interest to improve procedures for calculating efficiencies of the pressure-wave pattern for pressure relief. This would be especially desirable for times immediately after flame breakthrough, since such an improvement could eliminate the theoretical discontinuity in overpressure. Less uncertain approaches for taking into account upward expansion and buoyant rise of burnt gases also seem worth investigating. In addition, ignition and flame-development studies, directed toward obtaining improved effective values of the initial shock radius, seem warranted in view of the sensitivity of the predictions to this parameter. And, of course, better burning-velocity information will always be needed.

Finally, it would be of interest to attempt to extend the simplified models to account for configurations lacking axial symmetry. Although such extensions would probably involve introduction of significant additional uncertainties, they would enhance predictive capabilities for hazards of practical concern, in a realm for which finite-difference methods are generally unavailable. Moreover, they may uncover configurations particularly prone to flame acceleration.

I am especially indebted to Dave Lucas for many significant observations and suggestions concerning this work.

Appendix A. Efficiency of the shock pattern

First consider as a control volume a right circular cylinder of radius R and height h. The mass contained initially in this volume is $\pi\rho_0 R^2 h$, where ρ_0 is the initial density. When the shock radius is R the mass in this volume is $\pi\rho_2 r^2 h + \pi\rho_1(R^2 - r^2)\,h$, where ρ_2 and ρ_1 are respectively the average densities of the burnt gas and of the shocked but unburnt gas. If there were no upward relief then this mass would equal the initial mass. Because of relief through propagation of pressure waves above the cloud and through upward expansion, this mass is less than the initial mass. The efficiency η may be defined by stating that the difference between the initial mass and the actual mass at the time of interest is $\frac{2}{3}\pi\eta(\rho_1 - \rho_0)\,R^3$.

This definition may be motivated by considering a control volume consisting of

a hemisphere of radius R with a horizontal base located at the top of the previous control volume. Since buoyant rise of hot gas is much slower than shock propagation, non-combustible gas outside this hemisphere is uninfluenced by the explosion. Therefore mass conservation provides, as an equivalent definition of η,

$$\eta = \frac{\iiint(\rho-\rho_0)\,dV}{(\rho_1-\rho_0)V}, \tag{A 1}$$

where ρ is the local density and V is the volume of the hemisphere, the integration being extended over this volume. According to (A 1), η is the ratio of the volume-average overdensity in the hemisphere to the average overdensity of the shocked but unburnt gas.

For small Mach numbers of flame propagation, a well-posed acoustic problem can be defined for calculating the ρ-field and hence η. In this acoustic limit the hemispherical control volume corresponds properly to the region influenced by pressure waves. An idea of the magnitude of η can be obtained from approximate considerations that do not involve solution of the acoustic problem. For example, if the overdensity field is assumed to vary inversely with radius, then in the cylindrical region

$$\rho_1-\rho_0 \propto \frac{2\pi\int^R x^{-1}x\,dx}{2\pi\int^R x\,dx} = \frac{R}{\frac{1}{2}R^2},$$

while in the hemispherical region

$$\frac{\iiint(\rho-\rho_0)\,dV}{V} \propto \frac{2\pi\int^R x^{-1}x^2\,dx}{2\pi\int^R x^2\,dx} = \frac{\frac{1}{2}R^2}{\frac{1}{3}R^3},$$

with the same constant of proportionality. The value of η is then found from (A 1) to be $\frac{3}{4}$. As an opposite and unrealistic extreme that corresponds to a point source at time zero, it may be assumed that all of the overdensity is located in a shell at the edge of the region of disturbance; it is then found that

$$\eta = \frac{2\pi\int^R x^{-1}\delta(R-x)x^2\,dx \Big/ 2\pi\int^R x^2\,dx}{2\pi\int^R x^{-1}\delta(R-x)\,x\,dx \Big/ \pi R^2} = \tfrac{3}{2}.$$

If the shell of overdensity exists only above the cloud, and the density remains constant for the shocked but unburnt gas in the cylindrical control volume, then $x^{-1}\delta(R-x)$ is replaced by unity in the denominator, and $\eta = \frac{3}{4}$ is obtained. Although none of these estimates is definitive, all produce values of η of order unity. We conclude that $\eta = 0{\cdot}8$ may be used, with at least 20 % accuracy, for low Mach numbers of flame propagation.

Values of η appreciably greater than unity cannot be achieved without assigning the non-combustible gas a substantially greater capacity than the combustible for accepting mass under the influence of pressure waves. Smaller values of η would necessitate a reduced extent of the region of overdensity in the gas above the cloud; this may occur at high Mach numbers of flame propagation. Upward expansion of hot products of combustion reduces η by reducing the density in part of the hemisphere, but the fraction of the volume so affected is usually small compared with the total volume of the hemisphere.

Appendix B. Effects of upward expansion of hot gases

Both buoyancy and the volume increase associated with the density decrease during combustion tend to produce upward expansion of the burnt gas. At first let us neglect buoyancy, which becomes important only in late stages. During spherical propagation the gas expansion then is isotropic, and at the time that the flame breaks through the top of the combustible cloud the non-dimensional radius is $x = x_t$, where

$$x_t = \frac{\alpha}{(P\theta)^{\frac{1}{3}}}. \tag{B 1}$$

Thus the height of the cloud expands by a factor proportional to the cube root of the density ratio. This factor of expansion is necessary if the burnt gas is to remain at rest.

After breakthrough it seems reasonable to assume that the burnt gas continues to expand isotropically. If the burnt gas is approximated as a circular cylinder of radius r and height h_b, then

$$h_b = \frac{h}{(P\theta)^{\frac{1}{3}}} \tag{B 2}$$

is obtained for the burnt-cloud height. The influence of (B 2) on the mass balance for the burnt gas may be investigated by considering a cylindrical control volume of radius r and height h. The rate of upward motion of burnt gases out of this control volume may be expressed in terms of v, the average vertical velocity across the surface at height h. The mass balance for the control volume becomes

$$2\pi r h \rho_f S - \pi r^2 \rho_b v = \frac{d(\pi r^2 h \rho_b)}{dt}, \tag{B 3}$$

where ρ_b and ρ_f denote respectively the densities of the burnt gas and of the gas just ahead of the flame. Derivation of (6) from (B 3) necessitates introduction of an approximation for v.

If all of the upward expansion occurs just prior to the arrival of the flame, then there is no further upward expansion in the control volume considered, and $v = 0$. In this case the flame sheet extends to height h_b and has quiescent conditions behind it, and $\beta = 1$ in (6). The opposite limiting case is that in which all of the upward expansion occurs after arrival of the flame. In this case, since the burnt material occupies a cylinder of height h_b, the mass conservation is $2\pi r h \rho_f S = d(\pi r^2 h_b \rho_b)/dt$, which provides

$$v = \frac{2S\rho_f}{\rho_b} \frac{h}{r}\left(1 - \frac{h}{h_b}\right)$$

when substituted into (B 3), and gives $\beta = h/h_b$ in (6). The average of these two extremes provides

$$\beta = \tfrac{1}{2}[1 + (P\theta)^{\frac{1}{3}}] \tag{B 4}$$

when use is made of (B 2).

The radial component of velocity of the burnt gas just behind the flame, u_b, may be related to v by assuming steady flow (no mass accumulation) in the cylindrical control volume of height h which is terminated just behind the flame, namely $2\pi r h(-u_b)\rho_b = \pi r^2 v \rho_b$. By substituting into this formula half of the maximum estimate for v given above, we obtain

$$u_b = -\tfrac{1}{2} S \frac{\rho_f}{\rho_b}\left(1 - \frac{h}{h_b}\right) \tag{B 5}$$

as a rough estimate. The steady-flow approximation is best if the upward flow occurs mainly near the flame so that there is relatively little variation of burnt-cloud height with radius.

The general expression for mass conservation across the flame is

$$\rho_f S = \rho_b(S+u_f-u_b), \tag{B 6}$$

where u_f is the radial velocity of the gas just ahead of the flame. Use of (B5) in (B6) gives

$$u_f = S\left[\frac{1}{2}\frac{\rho_f}{\rho_b}\left(1+\frac{h}{h_b}\right)-1\right]. \tag{B 7}$$

There are evidently uncertainties in these estimates, and the alternative formula

$$u_f = \beta S\left[\frac{\rho_f}{\rho_b}-1\right], \tag{B 8}$$

which corresponds to

$$u_b = -S(1-\beta)\left[\frac{\rho_f}{\rho_b}-1\right], \tag{B 9}$$

appears to be just as good, and also produces some algebraic simplifications in the analysis.

Effects of buoyancy may be estimated by considering a vertical momentum balance for the cylindrical region of burnt gas with only inertial and gravitational forces included. This balance may be written as

$$\frac{d(\pi r^2 h_b \rho_b \bar{v})}{dt} = \pi r^2 h_b(\rho_f-\rho_b)g, \tag{B 10}$$

where $\bar{v}$ is the volume-average vertical component of velocity over the cylinder and g represents the acceleration due to gravity. From (B10) it is seen that buoyancy produces an increment in the vertical velocity of the burnt gas given roughly by $[\rho_f/\rho_b-1]gt$, where t denotes time from ignition. This increment may be added to v in (B3), and in the steady-flow approximation it provides an additional contribution of $-\frac{1}{2}(r/h)[\rho_f/\rho_b-1]gt$ to u_b, thereby increasing the horizontal inflow velocity behind the flame (and hence decreasing the outflow velocity ahead of it). The buoyancy correction is negligible at early times, but becomes large at late times for sufficiently flat clouds.

Appendix C. Momentum conservation for the shocked but unburnt gas

The necessary statement of momentum conservation may be derived, for example, by beginning with the differential forms of the conservation equations for mass and momentum with viscous and gravitational forces neglected. Integration of a suitable combination of these equations from the burnt gas just behind the flame (identified by subscript b) to the undisturbed gas just outside the shock gives

$$\frac{d}{dt}\int_r^R \rho u X^{j-1}\,dX = (\Delta p_b+\rho_b u_b^2)\,r^{j-1}+(j-1)\int_r^R \Delta p X^{j-2}\,dX, \tag{C 1}$$

where ρ denotes density, u radial velocity, Δp overpressure (the difference between the local pressure and ambient pressure) and X the radial coordinate.

In the last integral we replace Δp by the constant average overpressure $\overline{\Delta p} = bP+(1-b)p-1$, where the weighting factor b defines the importance of the pressure at the flame (in comparison with that at the shock) in contributing to the

average of Δp. It seems logical to take the arithmetic mean, $b = \frac{1}{2}$, but for the spherical problem, $j = 3$, this selection results in a non-physical prediction that $p < 1$ in the quasi-steady solution for small s. To avoid this inconsistency, the value $b = \frac{1}{4}j$ is employed; for $j = 3$ this ensures that $p > 1$ and causes $p-1$ to approach zero more rapidly than $P-1$ as s approaches zero.

The non-dimensional momentum is conveniently defined as

$$m = \int_r^R \frac{\rho}{\rho_0}\frac{u}{a_0}\frac{X^{j-1}\,dX}{R_0^j}, \tag{C 2}$$

where ρ_0 is the ambient density. With this definition and the pressure weighting just discussed, (C1) gives (7) directly when the momentum balance across the flame, $\Delta p_b = P-1-(s^2/K)[\rho_f/\rho_b-1]$, is employed.

A general approach to the definition of volume averages may be introduced to obtain an expression for m; this results in

$$m = [(1-a)\rho_s u_s R^{j-1} + a\rho_f u_f r^{j-1}]\frac{R-r}{\rho_0 a_0 R_0^j}, \tag{C 3}$$

where the subscript s identifies conditions just behind the shock and where a is the fraction of the contribution of the value of ρu at the flame to the average value of ρu. In (C3), mass conservation across the shock, $\rho_s(-u_s + dR/dt) = \rho_0\, dR/dt$, is employed to write

$$\frac{\rho_s u_s}{\rho_0 a_0} = \frac{[(p-1)(1-\kappa)]^{\frac{1}{2}}}{\kappa}, \tag{C 4}$$

where use has been made of (1). In addition, if (B8) is selected for u_f, then

$$\frac{\rho_f u_f}{\rho_0 a_0} = \frac{\beta s}{K}\left[\frac{1}{K\theta P}-1\right]. \tag{C 5}$$

Substitution of (C4) and (C5) into (C3) produces (8).

REFERENCES

Chiu, K. W., Lee, J. H. & Knystautas, R. 1977 The blast waves from asymmetrical explosions. *J. Fluid Mech.* **82**, 193–208.

Kuhl, A. L. 1981 Similarity analysis of flame-driven blast waves with real equations of state. In *Proc. First Specialists' Meeting (International) of The Combustion Institute*, pp. 491–496.

Williams, F. A. 1976 Qualitative theory of nonideal explosions. *Combust. Sci. Tech.* **12**, 199–206.